J Biol Inorg Chem (2002) 7: 897–908
DOI 10.1007/s00775-002-0379-6

ORIGINAL ARTICLE

Thorsten Buhrke · Marc Brecht · Wolfgang Lubitz
Bärbel Friedrich

The H_2 sensor of *Ralstonia eutropha*: biochemical and spectroscopic analysis of mutant proteins modified at a conserved glutamine residue close to the [NiFe] active site

Received: 1 March 2002 / Accepted: 4 May 2001 / Published online: 18 June 2002

Abstract [NiFe] hydrogenases contain a highly conserved histidine residue close to the [NiFe] active site which is altered by a glutamine residue in the H_2-sensing [NiFe] hydrogenases. In this study, we exchanged the respective glutamine residue of the H_2 sensor (RH) of *Ralstonia eutropha*, Q67 of the RH large subunit HoxC, by histidine, asparagine and glutamate. The replacement by histidine and asparagine resulted in slightly unstable RH proteins which were hardly affected in their regulatory and enzymatic properties. The exchange to glutamate led to a completely unstable RH protein. The purified wild-type RH and the mutant protein with the Gln/His exchange were analysed by continuous-wave and pulsed electron paramagnetic resonance (EPR) techniques. We observed a coupling of a nitrogen nucleus with the [NiFe] active site for the mutant protein which was absent in the spectrum of the wild-type RH. A combination of theoretical calculations with the experimental data provided an explanation for the observed coupling. It is shown that the coupling is due to the formation of a weak hydrogen bond between the protonated N(ϵ) nucleus of the histidine with the sulfur of a conserved cysteine residue which coordinates the metal atoms of the [NiFe] active site as a bridging ligand. The effect of this hydrogen bond on the local structure of the [NiFe] active site is discussed.

Keywords Hydrogen sensor · Regulatory hydrogenase · [NiFe] active site · Electron paramagnetic resonance · Electron spin echo envelope modulation

T. Buhrke · B. Friedrich (✉)
Institut für Biologie,
Humboldt-Universität zu Berlin,
Chausseestrasse 117,
10115 Berlin, Germany
E-mail: baerbel.friedrich@rz.hu-berlin.de
Tel.: +49-30-20938101
Fax: +49-30-20938102

M. Brecht · W. Lubitz
Max Volmer Laboratorium für Biophysikalische Chemie,
Institut für Chemie, Technische Universität Berlin,
Strasse des 17 Juni 135,
10623 Berlin, Germany

W. Lubitz
Max-Planck-Institut für Strahlenchemie,
Stiftstrasse 34–36,
45470 Mülheim/Ruhr, Germany

Introduction

Utilization of molecular hydrogen as an alternative energy source is a common metabolic trait of microorganisms. The reaction is catalyzed by hydrogenase, which mediates the reversible conversion of H_2 to $2H^+$ and $2e^-$. Metal-containing hydrogenases are classified into two major classes: the [NiFe] hydrogenases and the Fe-only hydrogenases (for review see [1]). X-ray structure analysis of [NiFe] hydrogenases from sulfate-reducing bacteria gave insights into the architecture of the heterodimer and uncovered an H_2-activating site consisting of a nickel and an iron atom deeply buried inside the large subunit [2, 3]. The two metals are coordinated via thiolates provided by four cysteine residues. Moreover, three diatomic nonprotein ligands are bound to the iron. Fourier transform infrared spectroscopy (FTIR) and chemical analysis of the *Allochromatium vinosum* [NiFe] hydrogenase identified one CO and two CN^- groups as the diatomic ligands [4, 5]. In the *Desulfovibrio vulgaris* Miyazaki F [NiFe] hydrogenase, one of the CN^- groups appears to be replaced by SO [3]. Finally, a bridging ligand between the nickel and the iron atom was observed in the X-ray structure of oxidized [NiFe] hydrogenases. This ligand was identified as an oxygen species (O^{2-} or OH^-) for the *D. gigas* enzyme [6]. For the *D. vulgaris* enzyme it was suggested to be a sulfur species [3].

Despite a great wealth of structural information, the catalytic mechanism of [NiFe] hydrogenases is still a matter of debate. The different redox states of the [NiFe] center can be resolved by electron paramagnetic resonance (EPR) spectroscopy (for a review see [7]). The as-isolated, oxidized hydrogenases usually show a

mixture of "ready" (Ni-B) and "unready" (Ni-A) forms. Both variants are paramagnetic and therefore EPR-detectable. The two forms can be converted by reductive activation of the enzyme to the EPR-silent Ni-S state. This conversion is obviously accompanied by the loss of the bridging ligand. Further reduction with H_2 results in the paramagnetic Ni-C state in which a hydride is bound to the [NiFe] center. The question of whether the hydride is bound to the nickel, or to the iron or even to both metals is still not solved. The catalytic cycle implies the transfer of electrons from the active site to the protein surface via iron-sulfur clusters located in the small subunit and the release of protons via a proton channel [8]. Hydrogen gas is considered to be transferred to the [NiFe] site via hydrophobic channels in the large subunit [9].

The proteobacterium *Ralstonia eutropha* harbors two energy-conserving [NiFe] hydrogenases, a membrane-bound enzyme which is coupled to the respiratory chain via a *b*-type cytochrome [10, 11], and a cytoplasmic soluble hydrogenase which confers the ability to directly reduce NAD^+ at the expense of H_2 [12, 13]. The structural genes for the two enzymes are arranged in two distinct operons, together with sets of accessory genes whose products are required for posttranslational maturation of the metal-containing enzymes [14].

H_2-dependent transcription of the two operons is directed by a signal transduction apparatus consisting of the response regulator HoxA and its cognate histidine protein kinase HoxJ. H_2 sensing is mediated by an additional third component, a regulatory hydrogenase (RH) [15] which forms a subclass of [NiFe] hydrogenases [16]. This H_2 sensor has also been found in other proteobacteria like *Rhodobacter capsulatus* [17] and *Bradyrhizobium japonicum* [18]. FTIR and EPR analysis of the H_2-sensing protein of *R. eutropha* revealed a standard type of active site [$NiFe(CO)(CN^-)_2$]. Further biochemical characterization uncovered a couple of uncommon biochemical features: the H_2-oxidizing activity of the RH is approximately two orders of magnitude lower than the activity of standard [NiFe] hydrogenases and is insensitive to inhibition by oxygen and carbon monoxide. The as-isolated RH does not require reductive activation prior to catalysis; it is present in the Ni-S and Ni-C states but lacks the Ni-A and Ni-B configurations [19, 20].

Provided the composition of the active site of H_2-sensing hydrogenases is identical to the standard type of [NiFe] hydrogenase, the RH-specific biochemical features may reflect differences in the protein composition in the environment of the [NiFe] active site. Currently, more than 100 DNA sequences of [NiFe] hydrogenases are available in the database. Five conserved motifs (L1 to L5) are obvious in the [NiFe] hydrogenase large subunits [7]. These highly conserved amino acid residues appear to be located close to the [NiFe] active site. Motif L2 (RxCGxCxxxH) comprises two of the four metal coordinating cysteines in addition to a histidine residue. Figure 1A shows a schematic

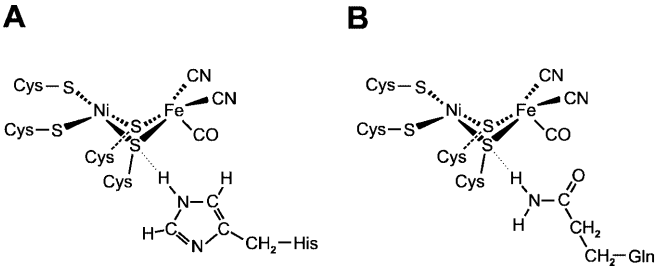

Fig. 1A, B. The active site of [NiFe] hydrogenases based on the crystal structure of the *D. gigas* enzyme [2]. **A** In the standard enzyme, a conserved histidine residue of the L2 motif is located in close vicinity to the bridging cysteine. **B** This histidine residue is replaced by a glutamine residue in the H_2 sensors

representation of the [NiFe] active site of the *D. gigas* enzyme. The histidine residue of motif L2 (His72) is in close vicinity to Cys533, a conserved cysteine residue that functions as a bridging ligand coordinating both the nickel and the iron atom of the [NiFe] active site [2]. This histidine residue is strictly conserved in the sequences of standard [NiFe] hydrogenases, but is altered by a glutamine residue in all H_2-sensing hydrogenases so far known (Fig. 1B) [16].

To see if this modification has any effect on the RH properties, we exchanged the respective glutamine (Gln67) of the RH large subunit HoxC of *R. eutropha* with histidine, asparagine and glutamate, respectively. The regulatory, biochemical and spectroscopic properties, including EPR and electron spin echo envelope modulation (ESEEM), of the mutant proteins are described.

Materials and methods

Strains and plasmids

The strains and plasmids used in this study are listed in Table 1. Strains with the initials HF were derived from *R. eutropha* H16. *Escherichia coli* JM109 [21] was used for standard cloning procedures, and *E. coli* S17-1 [22] was used for conjugative plasmid transfers between *E. coli* and *R. eutropha*.

The mutations in *hoxC* were generated by site-directed mutagenesis according to the method of Chen and Przybyla [23]. Plasmid pCH397 containing *hoxC* served as a template, and Vent DNA polymerase (New England Biolabs) was used for DNA amplification. 845-bp fragments were amplified from pCH397 by using the synthetic oligonucleotide 5′-GGAACCCGACGGACGCC-3′ as the nonmutagenic primer and the oligonucleotides 5′-GGCCGCG ACCGAgTGGGACACCGAGCAG-3′ (resulting in HoxC Q67H), 5′-GGCCGCGACCGAaTtGGACACCGAGCAG-3′ (resulting in HoxC Q67N) and 5′-GGCCGCGACCGACTc GGACACC-GAGCAG-3′ (resulting in HoxC Q67E), respectively, as the mutagenic primers (lowercase denotes exchanged bases). The PCR products and the synthetic oligonucleotide 5′-GTGAGGAAA-CATC GCAGG-3′ were used as primers in a second amplification step. 945-bp *Eco*RI fragments of the resulting 1336-bp PCR products were cloned into the *Eco*RI site of Litmus28, yielding pCH704 (HoxC Q67H), pCH705 (HoxC Q67N) and pCH706 (HoxC Q67E), respectively. The correctness of the amplified sequences was confirmed by sequencing. 1.1-kp *Sna*BI-*Stu*I fragments of these plasmids were cloned into the *Pme*I-site of suicide vector pLO2 to give pCH733 (HoxC Q67H), pCH734 (HoxC Q67N) and pCH735 (HoxC Q67E), respectively.

Table 1. Strains and plasmids

Strain or plasmid	Relevant characteristics	Source or reference
R. eutropha		
H16	Wild-type, SH^+ MBH^+ RH^+ $HoxJ^-$ (*hoxJ*g1264a)	DSM428, ATCC 17699
HF433	SH^+ MBH^+ RH^+	[15]
HF435	SH^+ MBH^+ RH^- (*hoxC*Δ)	[15]
HF559	SH^+ MBH^+ RH (HoxC Q67H)	This study
HF560	SH^+ MBH^+ RH (HoxC Q67N)	This study
HF561	SH^+ MBH^+ RH (HoxC Q67E)	This study
HF500	SH^- (*hoxH*Δ), MBH^- (*hoxG*Δ), RH^- (*hoxC*Δ), $HoxJ^-$ (*hoxJ*g1264a)	[16]
HF574	SH^- (*hoxH*Δ), MBH^- (*hoxG*Δ), RH^- (*hoxB*Δ*hoxC*Δ), $HoxJ^-$ (*hoxJ*g1264a)	This study
E. coli		
JM109	F′ *traD36 lacI*^{q}, Δ(*lacZ*)*M15 proA*$^+$ *B*$^+$/e14$^-$ ($McrA^-$) Δ(*lac-proAB*) *thi gyrA96 (Nal*^{r}*) endA1 hsdR17(rk*$^-$*mk*$^+$*) relA1 supE44 recA1*	[21]
S17-1	Tra^+ *recA pro thi hsdR*, *chr*:RP4-2	[22]
Plasmids		
LITMUS 28/29	Ap^r *lacZ′*, ColE1 *ori*	New England Biolabs
pLO2	Km^r, *sacB*, RP4 *oriT*, ColE1 *ori*	[24]
pEDY309	RK2 *ori*, Tc^r, Mob^+, promoterless *lacZ* gene	[16]
pCH397	pACYC177 with a 3.3-kb *Pst*I fragment containing *hoxBC*	[16]
pCH643	pLO2 with a 0.8-kb *Xmn*I-*Xho*I fragment containing *hoxB*Δ	[15]
pCH594	LITMUS 29 with a 2.8-kb *Hin*dIII-*Nco*I fragment containing P_{SH}-*hoxB-hoxC*	[16]
pCH704	LITMUS 28 containing a 945-bp *Eco*RI cut PCR product (HoxC Q67H)	This study
pCH705	LITMUS 28 containing a 945-bp *Eco*RI cut PCR product (HoxC Q67N)	This study
pCH706	LITMUS 28 containing a 945-bp *Eco*RI cut PCR product (HoxC Q67E)	This study
pCH733	pLO2 containing a 1.1-kb *Sna*BI-*Stu*I fragment of pCH704	This study
pCH734	pLO2 containing a 1.1-kb *Sna*BI-*Stu*I fragment of pCH705	This study
pCH735	pLO2 containing a 1.1-kb *Sna*BI-*Stu*I fragment of pCH706	This study
pCH861	Religated pCH594 after digestion with *Bam*HI and *Bgl*II	This study
pCH865	945-bp *Eco*RI fragment of pCH704 in *Eco*RI digested pCH861	This study
pCH866	945-bp *Eco*RI fragment of pCH705 in *Eco*RI digested pCH861	This study
pCH867	945-bp *Eco*RI fragment of pCH706 in *Eco*RI digested pCH861	This study
pGE301	Φ(*hoxK′-lacZ*), Tc^r	[24]
pGE377	pEDY309 with a 2.8-kb *Hin*dIII-*Xba*I fragment containing P_{SH}-*hoxB-hoxC*	[16]
pGE463	pEDY309 with a 2.9-kb *Hin*dIII-*Spe*I fragment of pCH865 (HoxC Q67H)	This study
pGE464	pEDY309 with a 2.9-kb *Hin*dIII-*Spe*I fragment of pCH866 (HoxC Q67N)	This study
pGE465	pEDY309 with a 2.9-kb *Hin*dIII-*Spe*I fragment of pCH867 (HoxC Q67E)	This study

For the overproduction of the modified RH proteins in *R. eutropha*, the mutations were introduced into plasmid pCH594 that contains a fusion of the SH promoter from *R. eutropha* with the RH structural genes *hoxBC* [16]. In a first step, the *Eco*RI site of the polylinker of pCH594 was eliminated by a *Bam*HI-*Bgl*II digest; subsequent religation yielded plasmid pCH861. Thereafter, the mutations were introduced by cloning the 945-bp *Eco*RI fragments of pCH704, pCH705 and pCH706 into the *Eco*RI-treated pCH861, yielding pCH865 (HoxC Q67H), pCH866 (HoxC Q67N) and pCH867 (HoxC Q67E), respectively. The 2.9-kb *Hin*dIII-*Spe*I fragments of these plasmids were cloned into the broad-host-range vector pEDY309 [16], digested with *Hin*dIII and *Spe*I to give pGE463 (HoxC Q67H), pGE464 (HoxC Q67N) and pGE465 (HoxC Q67E), respectively.

Media and growth conditions

E. coli strains were grown in Luria Broth (LB). *R. eutropha* strains were grown in modified LB medium containing 0.25% (w/v) sodium chloride (LSLB) or in mineral salts medium containing 0.4% fructose (FN) or a mixture (FGN) of fructose and glycerol [0.2% (w/v) each] [14]. Sucrose-resistant segregants of *sacB*-harboring strains were selected on LSLB plates containing 15% (w/v) sucrose [24]. Solid media contained 1.5% (w/v) agar. Antibiotics were used at the following concentrations: 350 μg kanamycin mL^{-1} and 15 μg tetracycline mL^{-1} for *R. eutropha*, and 25 μg kanamycin mL^{-1}, 15 μg tetracycline mL^{-1} and 100 μg ampicillin mL^{-1} for *E. coli*.

Conjugative plasmid transfer and gene replacement

Mobilizable plasmids were transferred from *E. coli* to *R. eutropha* using a spot mating technique. Gene replacement in *R. eutropha* was achieved by allelic exchange based on the conditionally lethal *sacB* gene [24]. The resulting isolates were screened for the presence of the desired mutation by PCR amplification of the respective target site [25]. Deletion-carrying isolates were identified by the altered electrophoretic mobility of the amplification products.

Mutations in the codon for Q67 in *hoxC* were introduced into *R. eutropha* HF433 by using suicide plasmids pCH733, pCH734 and pCH735 to give HF559 (HoxC Q67H), HF560 (HoxC Q67N) and HF561 (HoxC Q67E), respectively. Plasmid pCH643 containing *hoxB*Δ [15] was used to delete the gene for the RH small subunit HoxB in HF500, yielding HF574.

Purification of the RH

R. eutropha HF574 harboring either plasmid pGE377 or plasmid pGE463 was used for the purification of the wild-type and mutated RH proteins. Large-scale cultivation, cell disruption and protein purification was carried out as previously described [20]. As a final step, the purified proteins were dialysed against 10 mM Tris-HCl buffer (pH 8.0) and concentrated by ultrafiltration (Centriprep-10; Amicon). The protein solutions were transferred to an EPR tube. The enzymes were activated in the tube for 30 min at room temperature with 100% H_2 under frequent stirring and then the samples were rapidly frozen in liquid nitrogen.

Immunoblot analysis

Soluble protein fractions of *R. eutropha* were separated by SDS-PAGE on 12% gels and subsequently transferred to Protran BA85 nitrocellulose membranes (Schleicher and Schüll, Dassel, Germany) following a standard protocol [26]. The RH subunits HoxC and HoxB were identified using anti-HoxC serum, diluted 1:1000, and anti-HoxB serum, diluted 1:10,000, respectively, in addition to alkaline-phosphatase-labelled goat anti-rabbit IgG (Dianova, Hamburg, Germany).

Enzyme assays

H_2-oxidizing activity was quantified by an amperometric H_2-uptake assay as described previously using a H_2 electrode with methylene blue as the electron acceptor [19]. One unit of H_2-methylene blue oxidoreductase activity was the amount of enzyme which catalyzed the consumption of 1 μmol H_2 per min. D_2/H^+ exchange activity was determined as described in Bernhard et al. [20]. β-galactosidase activity was determined as described previously [27], and the activities were calculated according to Miller [28] with the modification that the cell density was measured at 436 nm. Protein of soluble extracts was determined according to the protocol of Lowry et al. [29].

Instrumentation

The EPR measurements were carried out on a commercial Bruker ESP 380E FT-EPR spectrometer equipped with a dielectric ring resonator (ESP 380-1052 DL Q-H). Resonator and sample were cooled with a helium flow-cryostat (Oxford CF 935). Simulations of the EPR spectra were done by using the program ELSI [30]. For the ESEEM (microwave pulse sequence $\pi/2$-τ-$\pi/2$-T-$\pi/2$) spectra, whole 2D data sets (32×256 points) were recorded. Hyperfine Sublevel Correlation (HYSCORE) [31] ($\pi/2$-τ-$\pi/2$-T_1-π-T_2-$\pi/2$) spectra were recorded for different values of τ with a resolution of 256×256 points for T_1 and T_2. In both cases we used a four-step phase cycle, described by Gemperle et al. [32]. The spectra were obtained, after baseline correction and multiplication with a Hamming function, from fast Fourier transform (FFT) (for ESEEM) or 2D-FFT (for HYSCORE).

Evaluation of spectra

Our spectra were analyzed based on a spin Hamiltonian of the following form ($S=1/2$, $I=1$) [33, 34]:

$$H = \mu_B \mathbf{B_0 g \hat{S}} + g_n \mu_n \mathbf{B_0 \hat{I}} + \mathbf{\hat{S} A \hat{I}} + \mathbf{\hat{I} P \hat{I}} \quad (1)$$

The first two terms describe the electron and the nuclear Zeeman interaction in which $\mathbf{B}_0$ is the external field, $\hat{\mathbf{S}}$ and $\hat{\mathbf{I}}$ are the electron and nuclear spin operators, μ_B and μ_n the Bohr and nuclear magneton, g_n is the nuclear g factor and $\mathbf{g}$ the electronic $\mathbf{g}$ tensor. The third term in Eq. 1 characterizes the hyperfine (hf) interaction, with $\mathbf{A}$ being the hf coupling (hfc) tensor. In the fourth term, $\mathbf{P}$ is the nuclear quadrupole coupling tensor [35].

The local magnetic field at the nucleus is directly proportional to frequencies $\nu_{\mathrm{eff}}^{\pm} = |\nu_n \pm |A|/2|$ with the nuclear Zeeman frequency $\nu_n = g_n \mu_n B_0/h$ [33]. For a hf coupling $|A| = 2\nu_n$, the local magnetic field is zero in one m_S state. This is called the *cancellation* condition and results in a reduction of the nuclear Hamiltonian H_n to a pure quadrupole interaction [33, 36]. In pulse EPR spectra (three- and four-pulse ESEEM) [34], three sharp lines can then be detected resulting from the zero field nuclear quadrupole transitions ν_0, ν_- and ν_+. From these, the components of the traceless quadrupole tensor P_i (frequency units) can be obtained:

$$\begin{aligned} P_1 &= 1/3(\nu_+ + \nu_-) = K(\eta - 1) \\ P_2 &= 1/3(\nu_+ - 2\nu_-) = -K(\eta + 1) \\ P_3 &= 1/3(\nu_- - 2\nu_+) = 2K \end{aligned} \quad (2)$$

which are related to the quadrupole coupling $e^2qQ/h = 4K$ and the asymmetry parameter $\eta = (q_{xx} - q_{yy})/q_{zz}$. Here, Q is the scalar nuclear quadrupole moment and eq_{ii} are the components ($i = x, y, z$) of the electric field gradient at the nucleus [37]. From an evaluation of these parameters, e^2qQ/h and η, a detailed picture of the bonding situation of the considered nucleus can be obtained [37].

The cancellation condition is not stringent; the three zero-field transitions can be observed experimentally in ESEEM spectra provided the relation $|\nu_n \pm |A|/2| < K$ is fulfilled for one m_S state [34]. Following Eq. 2, the determination of the nuclear quadrupole resonance (NQR) parameters from the zero-field frequencies is straightforward. If the cancellation condition is satisfied, the second m_S manifold is usually in the high-field regime. In the experimental spectrum this causes a double-quantum transition ($\Delta m_I = 2$) occurring at:

$$\nu_{\mathrm{dq}}^{+} = 2\left[(\nu_n \pm |A|/2)^2 + \zeta^2\right]^{1/2}, \quad \zeta = K\left(3 + \eta^2\right)^{1/2} \quad (3)$$

from which the effective hyperfine coupling (hfc) $|A|$ can be determined [34]. Both the isotropic and, if present, also the anisotropic part of the hfc contribute to $|A|$.

Computational details

All density functional theory (DFT) calculations on the hydrogenase model were performed using the GAUSSIAN 94 package [38]. Geometry optimization was carried out with Becke's three-parameter hybrid functional B3LYP [39] using a Pople-type basis set 6-31G* [40, 41]. Based on this optimized structure, calculations of the electric field gradient were performed with Becke's three-parameter hybrid functionals B3LYP and B3PW91 using a Pople-type basis 6-311 + G(df,pd) and 6-311 + G(3df,2pd). A calibration of eQ/h of ^{14}N for the 6-311 + G(df,pd) basis set was done by Bailey [42] and yielded 4.5617 ± 0.0043 MHz/a.u.

Results

H_2-sensing function of RH site-directed mutant proteins

The residue Gln67 located in the conserved L2 motif of the RH large subunit HoxC was replaced by histidine, asparagine and glutamate, respectively, using standard techniques for site-directed mutagenesis [23]. The modified alleles were introduced into the H_2-responding recipient HF433 of *R. eutropha* by double recombination, yielding strains HF559 (HoxC Q67H), HF560 (HoxC Q67N) and HF561 (HoxC Q67E), respectively. To examine whether the modified RH proteins were still capable of sensing molecular H_2 and in turn activating the transcription of the hydrogenase regulon, we introduced plasmid pGE301, carrying the *lacZ* reporter gene fused to the promoter of the membrane-bound hydrogenase operon, into each mutant strain. β-galactosidase activity was monitored with cells grown in fructose-glycerol minimal medium with and without H_2. Exchanges of Gln67 to histidine (HoxC Q67H) and asparagine (HoxC Q67N) decreased the H_2-induced level of β-galactosidase by 10% (Fig. 2, lane 3) and 25% (Fig. 2, lane 4), respectively. Mutant HF561 (HoxC Q67E) had completely lost the ability to respond to H_2 (Fig. 2, lane 5); its phenotypic behaviour resembled that of a strain carrying a deletion in *hoxC* (Fig. 2, lane 2).

Biochemical properties of the modified proteins

The RH in the wild-type strain of *R. eutropha* is expressed poorly and displays a low enzymatic activity [19, 20]. Therefore we took advantage of a plasmid-based overexpression system specifically developed for *R. eutropha* [16]. This system employs the broad-host-range plasmid pGE377 harboring the RH structural genes *hoxBC* under the control of the strong soluble hydrogenase promoter (P_{SH}). The mutated alleles, carrying the respective codon exchanges for Gln67, were introduced into *hoxC* of plasmid pGE377 (see Materials and methods), and the resulting recombinant plasmids were transferred from *E. coli* into *R. eutropha* HF574. This recipient strain is impaired in all three hydrogenases (RH^-, SH^-, MBH^-) due to deletions in the respective subunit genes (Table 1). The hydrogenase-free background provided the basis for excluding interferences between the host hydrogenases and the introduced plasmid-encoded RH mutant proteins.

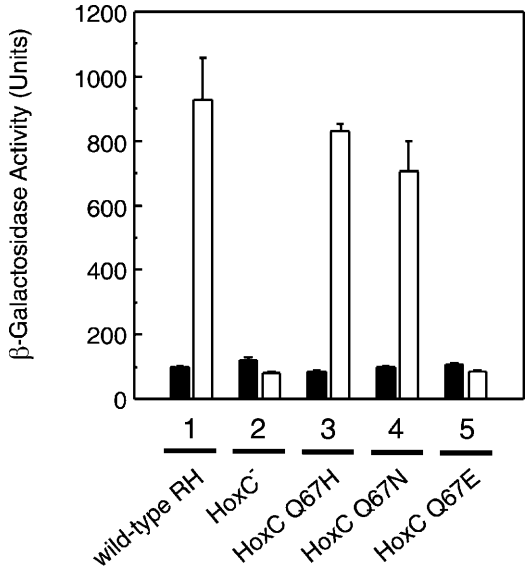

Fig. 2. H_2-sensing function of RH proteins modified in the Gln67 residue of the large subunit HoxC. Cells of *R. eutropha* strains harboring the plasmid-based Φ(*hoxK′-lacZ*) fusion were grown in fructose-glycerol minimal medium in the absence (*black bars*) and in the presence (*open bars*) of hydrogen. Cells were harvested at an OD(436 nm) of 8.0 ± 0.3 and the *β*-galactosidase activity was determined according to the protocol of Miller [28]. *Lane 1*, HF433; *lane 2*, HF435; *lane 3*, HF559; *lane 4*, HF560; *lane 5*, HF561

Transconjugant cells were cultivated in fructose-glycerol minimal medium, under conditions which allow high level expression of the SH promoter. The H_2-oxidizing activity was determined amperometrically with soluble extracts using methylene blue as the electron acceptor. The exchanges of Gln67 in HoxC to His and Asn, respectively, resulted in a 60 to 51% decrease of the specific activity (Table 2). A complete knockout of the H_2-oxidizing activity was observed for the third RH mutant (HoxC Q67E).

A similar activity pattern was obtained using the D_2/H^+ exchange assay, which allows determination of hydrogenase activity independently of electron transfer processes. The RH activity levels of the HoxC Q67H and HoxC Q67N mutant proteins showed a decrease of 66 and 28%, respectively (Table 2). Only H_2 production but no HD formation was detectable, as observed for the wild-type protein [20]. In agreement with the amperometric data, the RH (HoxC Q67E) mutant protein was completely devoid of D_2/H^+ exchange activity. Thus, the enzymatic activities of the mutant proteins correlated with their regulatory deficiencies.

To test whether the mutant proteins were stably expressed, soluble extracts were analysed for the presence of HoxB and HoxC antigen. The amount of RH detected in mutants carrying the HoxC Q67H and HoxC Q67N proteins was lower than in the wild type (Fig. 3, lanes 3 and 4). Since differences on the transcriptional level can be excluded, we assume that the mutant protein might be more sensitive to proteolytic degradation due to misfolding. No immunochemical reaction was identified in extracts from the HoxC Q67E strain, which suggests that this protein, once translated, immediately becomes degraded (Fig. 3, lane 5).

Preparation of RH proteins for spectroscopic analysis

Of the two mutants which formed stable RH proteins, the HoxC Q67H derivative was selected for detailed spectroscopic analysis. The conversion of Gln67 to His restored exactly the conserved L2 motif of standard [NiFe] hydrogenases. Thus, this RH derivative should be

Table 2. Enzymatic activities of the RH proteins in soluble extracts of *R. eutropha*

Strain	Relevant characteristic	Specific activity[a] (mU/mg of protein)	
		H_2-oxidizing activity[b]	D_2/H^+ exchange activity[c]
HF574(pGE377)	Wild-type RH	19.2	60
HF574(pEDY309)	$HoxC^-$	< 0.1	< 1
HF574(pGE463)	HoxC Q67H	7.7	20
HF574(pGE464)	HoxC Q67N	9.4	43
HF574(pGE465)	HoxC Q67E	< 0.1	< 1

[a]The values are the mean of two independent experiments
[b]H_2-oxidizing activity was determined amperometrically with methylene blue as electron acceptor
[c]D_2/H^+ exchange assays were carried out as described previously [20]

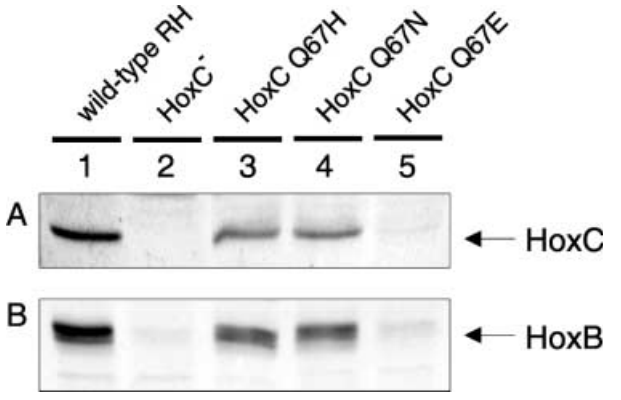

Fig. 3. Protein stability of the RH site-directed mutant proteins. RH-overproducing *R. eutropha* strains were grown in fructose-glycerol minimal medium under hydrogenase-derepressing conditions. The presence of the RH subunits HoxC and HoxB in soluble extracts was analyzed by standard immunoblot techniques. 20 µg of protein was applied to each lane. *Lane 1*, HF574(pGE377); lane 2, HF574(pEDY309); *lane 3*, HF574(pGE463); *lane 4*, HF574 (pGE464); *lane 5*, HF574(pGE465)

most appropriate for a direct spectroscopic comparison with standard [NiFe] hydrogenases.

Cells of *R. eutropha* strains HF574(pGE377) and HF574(pGE463) producing the wild-type and the mutant (HoxC Q67H) RH proteins, respectively, were cultivated in fructose-glycerol minimal medium on a 50-L scale. Protein purification from soluble extracts included heat treatment and chromatography via hydrophobic interaction and anionic exchange [20]. Starting with 95 g of cells (wet weight) of HF574(pGE377) yielded 3.7 mg of purified wild-type RH with a specific H_2-methylene blue oxidoreductase activity of 0.44 units/mg of protein. Starting with 90 g of cells (wet weight) of HF574(pGE463) yielded 3.65 mg of HoxC Q67H mutant protein with a specific activity of 0.174 units/mg of protein.

EPR spectroscopy

The protein solutions were transferred to EPR tubes, incubated with H_2 for 30 min at room temperature and then rapidly frozen in liquid nitrogen. We recorded EPR spectra of the wild-type RH and the RH (HoxC Q67H) protein at different temperatures, down to 5 K, and obtained spectra typical for the so-called Ni-C state found in standard hydrogenases [43, 44][1] as documented for the wild-type RH [19, 20]. This signal is characterized by spectral features from which the three **g** tensor principal values g_1, g_2 and g_3 are obtained. A second paramagnetic species was not detected in the RH proteins. Thus the [4Fe-4S] clusters obviously remained in their oxidized, diamagnetic states upon reduction of the

[1]From EPR studies of Ni-C in single crystals of the [NiFe] hydrogenase from *D. vulgaris* Miyazaki F (Foerster S, Stein M, Brecht M, Ogata H, Higuchi Y, Lubitz W, unpublished results)

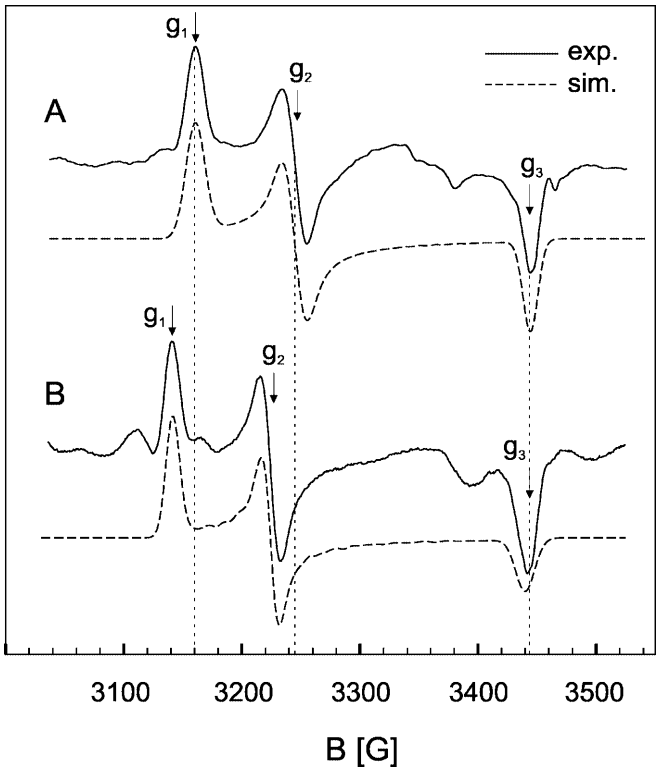

Fig. 4. EPR spectra and simulations of the Ni-C state of the wild-type RH (**A**) and the RH (HoxC Q67H) protein (**B**). For **g** tensor values, see Table 3. Experimental conditions: $T = 40$ K, modulation amplitude = 5 G, modulation frequency = 100 kHz, microwave frequency $\nu_{MW} = 9.71$ GHz, microwave power $P_{MW} = 1$ mW

hydrogenase with hydrogen. The EPR spectrum and simulation of the Ni-C signal in wild-type RH is shown in Fig. 4A, that of the RH (HoxC Q67H) protein in Fig. 4B. The spectra are similar to the Ni-C signal obtained from the wild type (Table 3). Whereas the **g** tensor components g_3 are identical within the error, g_1 and g_2 of the RH (HoxC Q67H) protein are slightly shifted compared to the wild-type RH. The component linewidths in the spectra are also not identical, indicating either *g* strain or differences in unresolved hf contributions (see below). Both spectra contain minor contributions from some other paramagnetic species. The **g** tensor values obtained from the simulations are collected in Table 3.

ESEEM spectroscopy

Pulsed EPR techniques like ESEEM and HYSCORE are sensitive methods for the detection of weak interactions between paramagnetic metal centers and insensitive nuclei in their surrounding such as ^{14}N or ^{2}H. The spectra yield information about the interaction strength via the magnitude of the hyperfine coupling and about the electric field gradient at the nucleus via the nuclear quadrupole coupling. Figure 5A shows an ESEEM spectrum of the Ni-C state of the wild-type RH, recor-

Table 3. Comparison of **g** tensor principal values of the Ni-C state of the wild-type RH and the RH (HoxC Q67H) protein from *R. eutropha* with the *g* values of the Ni-C state of standard [NiFe] hydrogenases

	g_1	g_2	g_3	Ref
Wild-type RH[a]	2.197 ± 0.003 (16 ± 1 G)	2.139 ± 0.003 (16 ± 2 G)	2.015 ± 0.003 (11 ± 1 G)	This study
RH(HoxC Q67H)[a]	2.209 ± 0.003 (11 ± 1 G)	2.152 ± 0.003 (11 ± 1 G)	2.016 ± 0.005 (16 ± 4 G)	This study
D. vulgaris Miyazaki F	2.198 ± 0.002	2.142 ± 0.002	2.012 ± 0.002	Unpublished results[b]
D. gigas	2.194	2.142	2.012	[43]
Allochromatium vinosum	2.19	2.15	2.01	[44]

[a]The respective linewidths are given in parentheses
[b]Foerster S, Stein M, Brecht M, Ogata H, Higuchi Y, Lubitz W

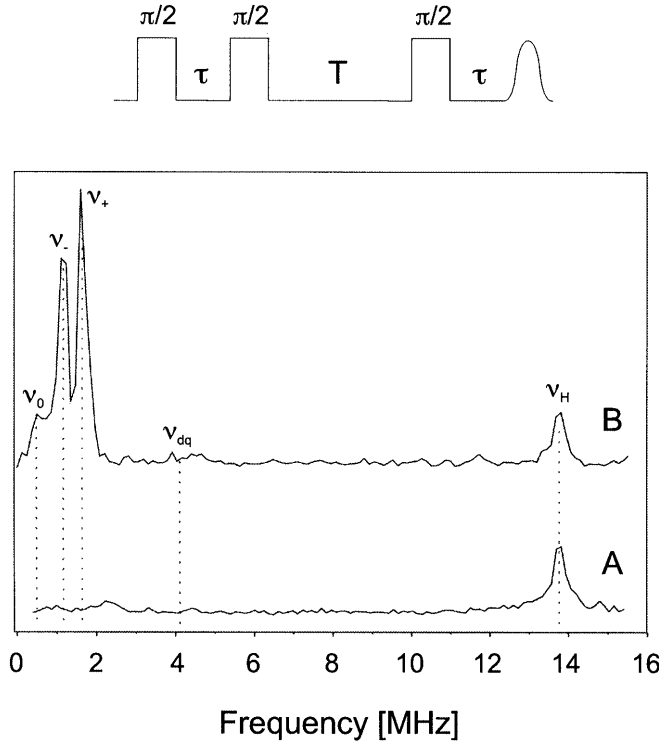

Fig. 5. Three-pulse ESEEM spectra of the wild-type RH (**A**) and the RH (HoxC Q67H) protein (**B**). Spectra were recorded at $g_2 = 2.14$ (see Fig. 4). For quadrupole parameters, see Table 4. Experimental conditions: $T = 6$ K, $\nu_{MW} = 9.71$ GHz, $\pi/2$ pulse = 8 ns, repetition rate = 30 Hz, resolution 256×32 points. *Top*: three-pulse microwave sequence used in the experiment

ded at $g_2 = 2.14$, corresponding to the maximum of the EPR absorption envelope (Fig. 5). It shows only one pronounced resonance at $\nu_H = 13.9$ MHz, arising from weakly coupled protons that occur near the nuclear Larmor frequency ν_H. Strongly coupled proton nuclei present in the system have a lower line intensity since the method is less sensitive for large proton couplings [34]. At other field positions of the EPR we obtained the same results, only ν_H is shifted according to the different nuclear Zeeman term (Eq. 1). Figure 5B shows the ESEEM spectrum of the Ni-C state of the RH (HoxC Q67H) protein also recorded at the g_2 component of the EPR signal. In addition to the proton line at ν_H, this ESEEM spectrum shows three lines at 0.48, 1.12 and 1.57 MHz (error: ±0.03 MHz) and a broad, poorly resolved feature near 4 MHz. These transitions can be attributed to zero-field quadrupole transitions (ν_0, ν_-, ν_+) and a double quantum transition (ν_{dq}) typical for a weakly coupled ^{14}N nucleus [33]. From the sharp lines we obtained the quadrupole coupling $e^2qQ/h = 1.8$ MHz and the asymmetry parameter $\eta = 0.53$, according to Eq. 2.

Owing to the weak double-quantum transition and the low resolution of the ESEEM spectrum, the value for ν_{dq} is not very accurate. However, using the HYSCORE technique we were able to resolve this transition. Figure 6 shows a HYSCORE spectrum of the RH (HoxC Q67H) protein, taken at the same field position as the ESEEM spectrum. In such a two-dimensional spectrum the off-diagonal peaks indicate correlations between the quadrupole transitions ν_0, $\nu_\pm$ and the double quantum transition (ν_{dq}). Sometimes, correlations with the single quantum transition ν_{sq} can also be detected. At the contour level chosen, the HYSCORE spectrum shows a well-resolved correlation peak between the ν_+ and the ν_{dq} transition. From $\nu_{dq} = 4.0$ MHz (error: ±0.1 MHz) we obtain from Eq. 3 an effective hyperfine coupling of $A_{eff} = 1.7$ MHz, which is close to the exact cancellation condition for ^{14}N [$2\nu(^{14}N) = 2.0$ MHz].

DFT calculations of quadrupole coupling constants

It has been shown that DFT calculation can accurately reproduce the geometry of molecules over a wide range of complexity [40]. These methods are also able to provide quite accurately the electric field gradient at the site of the different nuclei [42, 45, 46]. Inspection of the crystal structure of the [NiFe] hydrogenase of *D. gigas* [2] shows that the closest nitrogen nucleus to the nickel atom is the N(ϵ) of His72 of the large subunit. This histidine might be in contact with the bridging cysteine (Cys533) of the [NiFe] center via a hydrogen bond.

To prove this, we performed DFT calculation on a model system adopted from the X-ray structure consisting only of a CH_3CH_2SH group, taken from the

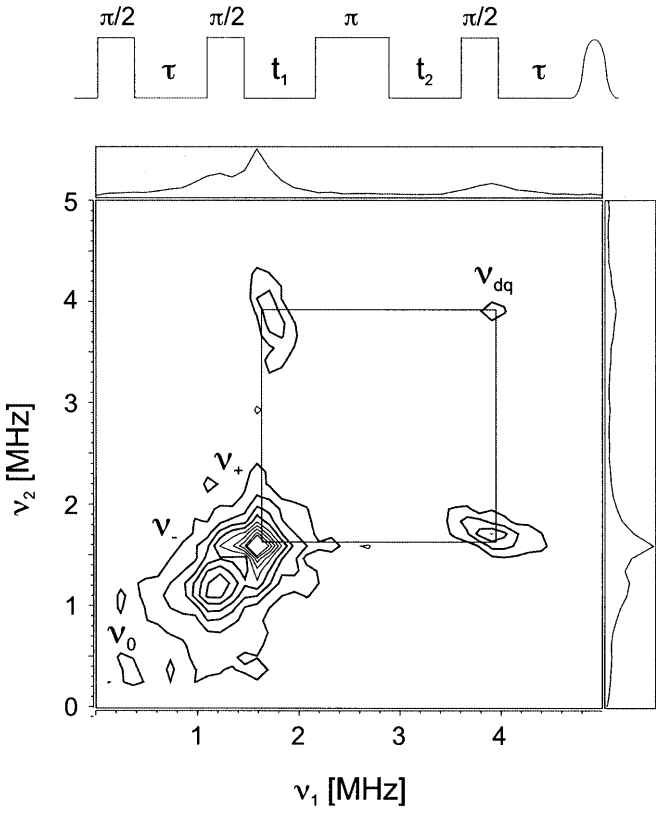

Fig. 6. Sum of two four-pulse ESEEM (HYSCORE) spectra of the RH (HoxC Q67H) protein. Spectra were recorded at $g_2 = 2.14$ with two different τ values. Experimental conditions: $T = 5$ K, $\nu_{MW} = 9.71$ GHz, $\pi/2$ pulse = 8 ns, $\tau = 120$ ns and 200 ns; starting values $t_1 = t_2 = 200$ ns, repetition rate 30 Hz, resolution 256×256 points, total collection time 35 h. *Top*: four-pulse microwave sequence used in the experiment

coordinates of Cys533 and the histidine residue of His72. The relative orientation of these residues and the distance between N(ϵ) of His72 and S of Cys533 was fixed during the geometry optimization. Note that the effect on the electric field gradient determining the ^{14}N nuclear quadrupole coupling (NQC) is mainly caused by the immediate surrounding of the nucleus. Thus, effects from the Ni and Fe (including their spin states) can be neglected to first order. Calculations of the ^{14}N NQC on the full system {model of the entire [NiFe] center [NiFe(CO)$(CN^-)_2$ moiety coordinated by four cysteine residues] to which the histidine, protonated at N(ϵ), is attached} yielded the following NQR parameters: $e^2qQ/h = 2.18$; $\eta = 0.30$ [57]. These values are nearly identical to those obtained by the simplified model used in this study (Fig. 7A). The NQR parameters e^2qQ/h and η can then be calculated for the geometry optimized model system. A plot of e^2qQ/h versus η allows the comparison of the experimental data with theoretical values.

We calculated the NQR parameters of the ^{14}N nuclei for a neutral histidine residue with different positions of the proton [protonation either of the N(ϵ) or the N(δ) position of the histidine residue] and for the double protonated case [protonation of both the N(ϵ) and N(δ) position]. To monitor the dependence of the NQR parameters on the distance d(N(ϵ)-S) between the N(ϵ) of the histidine and the sulfur of the cysteine, we calculated the NQR parameters e^2qQ/h and η for different distances (2.90–3.25 Å) for all protonation states of the histidine.

The results of the DFT calculations are in good agreement with the experimental data only for the case that N(ϵ) is protonated (Fig. 7A). We obtained a clear dependence of the NQR parameters of N(ϵ) (red triangles) on the distance d(N(ϵ)-S). Control calculations revealed that the NQR parameters of N(δ) (blue triangles) were not affected by the distance d(N(ϵ)-S). The experimentally determined NQR parameters for the RH (HoxC Q67H) protein (green square) almost match the calculated values for a N(ϵ)-S distance of 3.01 Å, while the experimental data for the *D. vulgaris* enzyme in the Ni-C state (black square) is in good agreement with the calculated values for a N(ϵ)-S distance of 3.08 Å. Thus, we could assume a slightly smaller N(ϵ)-S distance in the RH (HoxC Q67H) protein than in *the D. vulgaris* enzyme.

Based on our DFT calculations, we can exclude the possibility that N(δ) and not N(ϵ) of the histidine is protonated. For this case, the calculated NQR values do not match the experimental data (Fig. 7B). For the double protonated case (Fig. 7C) we again obtained a dependence of the calculated NQR parameter of N(ϵ) on the N(ϵ)-S distance. However, these values are in less good agreement to the experimental data than those obtained for the single protonated case (Fig. 7A).

Discussion

The mechanism of H_2 activation in the catalytic cycle of [NiFe] hydrogenases is currently investigated by spectroscopic techniques as well as by theoretical calculations in a number of laboratories. The H_2-sensing [NiFe] hydrogenase of *R. eutropha* exhibits a couple of particularly interesting features which make this protein an attractive object for detailed studies. FTIR and EPR spectroscopic data obtained for the wild-type RH indicate that this protein contains a [NiFe] active site of the standard NiFe(CO)$(CN^-)_2$ composition [19, 20]. Nevertheless, biochemical characteristics, such as the low enzymatic activity, insensitivity of the reaction to CO and O_2 inhibition and no requirement for reductive activation of the RH, point to significant alterations linked to the protein environment of the [NiFe] active site.

The [NiFe] center is embedded in a cavity formed by five conserved motifs (L1–L5) of the hydrogenase large subunit [7]. Only motifs L1 (RGxE) and L5 (DPCxxCxxH/R) are strictly conserved in all sequences of [NiFe] hydrogenases including the H_2 sensors, whereas significant alterations were found in the other motifs of the H_2 sensors [16]. The conserved proline residue of motif L4 (Gx_4PRGx_3H) is replaced by an alanine in the sequences of the H_2-sensing hydrogenases. Only two histidine residues of motif L3

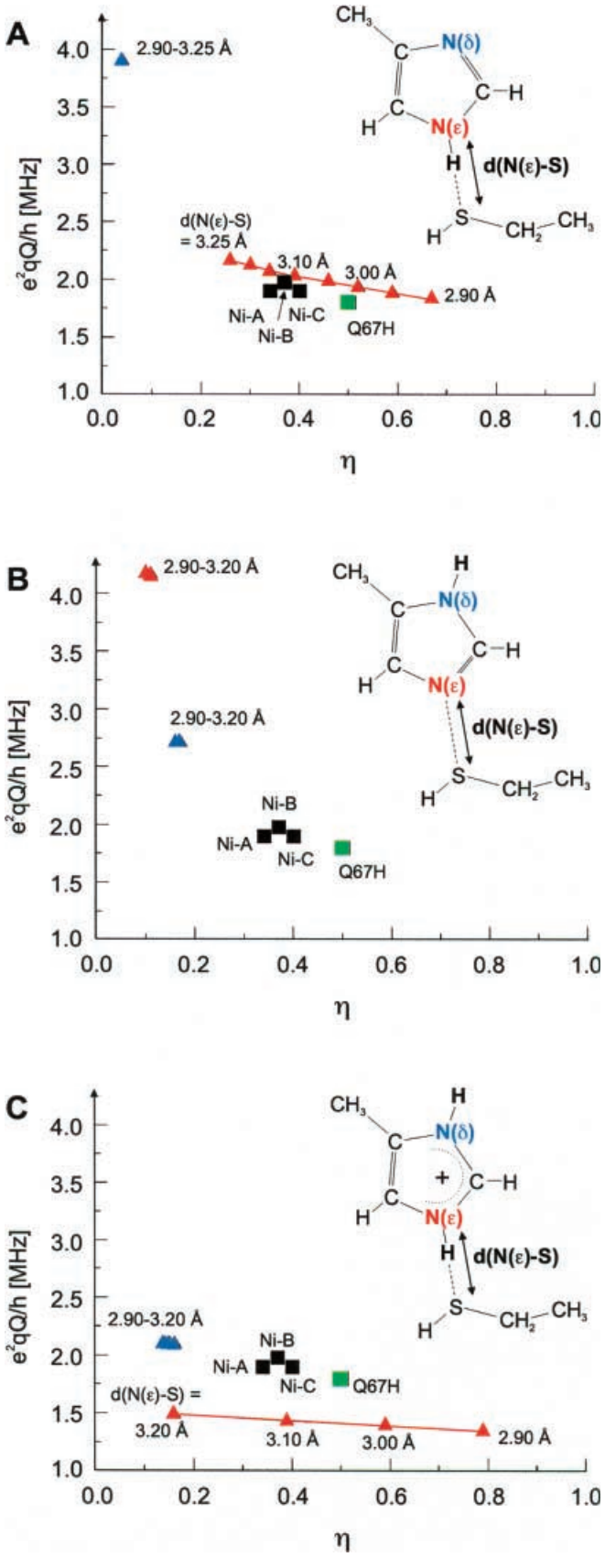

◀

Fig. 7A–C. Comparison of the NQR parameters from DFT calculations with experimental results from ESEEM measurements of the hydrogenase from *D. vulgaris* Miyazaki F and of the RH (HoxC Q67H) protein. For the DFT calculations, a model consisting of a histidine and a cysteine residue was used adopted from the X-ray structure of the *D. gigas* [NiFe] hydrogenase [2]. Plots of the NQR parameters (e^2qQ/h values versus the asymmetry parameter η) are shown for the cases when: **A** N(ϵ) of the histidine is protonated; **B** N(δ) of the histidine is protonated; **C** both N(ϵ) and N(δ) are protonated. *Red triangles* denote NQR parameters of N(ϵ); *blue triangles* denote NQR parameters of N(δ). The distances d(N(ϵ)-S), for which the NQR parameters were calculated, are given in the figure in Å. The experimentally determined NQR parameter of the Ni-A, Ni-B and Ni-C states of the [NiFe] hydrogenase of *D. vulgaris* Miyazaki F (*black squares*) and of the Ni-C state of the RH (HoxC Q67H) protein (denoted as "Q67H", *green square*) are included in each figure for comparison. Furthermore, each figure contains a schematic representation of the model used for the DFT calculations. The nitrogen nuclei N(ϵ) and N(δ) of the histidine are represented in *red* and *blue colors*, respectively, and the respective protons bound to the nitrogen and the distance d between N(ϵ) and the sulfur of the cysteine are highlighted (*boldface*)

(HxHxxHxxHLHxL) were found in the sequences of the H_2 sensors, but the residues of motif L3 are not strictly conserved in the standard enzymes as well. The most striking alteration was identified in motif L2 (RxCGxCxxxH). The histidine residue of motif L2 is strictly conserved in all sequences of [NiFe] hydrogenases with the exception of the H_2-sensing enzymes which carry a glutamine residue at this position. The conserved histidine residue is considered to participate in proton transfer, channeling the protons derived by the oxidation of H_2 to the protein surface [2].

In this study we focused our attention on the glutamine residue of motif L2 in the H_2-sensing hydrogenases. Glutamine at position 67 of the RH large subunit HoxC was replaced by histidine and asparagine, respectively. The resulting mutants displayed only a moderate phenotypic response. The regulatory activity of the RH was scarcely affected and the H_2-oxidizing activity in case of the purified RH (HoxC Q67H) protein was decreased to 40% compared to the wild-type RH. A conversion of Gln67 to glutamate, however, resulted in a completely unstable RH protein which could no longer be traced immunologically. This observation indicates that Gln67 is critical for the structural stability of the RH. A negatively charged residue at this position is obviously deleterious for the integrity of the RH protein.

In a previous study, the significance of the histidine residue of motif L2 was investigated for the SH of *R. eutropha*. The exchange of the histidine at position 69 in HoxH, the SH large subunit, to leucine resulted in an unstable SH protein with only residual enzymatic activity [47]. A stable SH protein was formed by the exchange of His69 to glutamine. However, the H_2-oxidizing activity of the SH (HoxH H69Q) protein was significantly reduced to a level of 20% compared to the wild-type SH (Burgdorf T, Friedrich B, unpublished results). This observation in fact points to a functional

Table 4. Comparison of the ^{14}N quadrupole parameters e^2qQ/h and η measured by ESEEM for different [NiFe] hydrogenases

Species	State	ν_0 (MHz)	ν_- (MHz)	ν_+ (MHz)	ν_{dq} (MHz)	e^2qQ/h (MHz)	η	Ref
RH (HoxC Q67H)	Ni-C	0.48 ± 0.04	1.12 ± 0.04	1.57 ± 0.02	4.0 ± 0.1	1.79 ± 0.04	0.53 ± 0.06	This work
D. vulgaris	Ni-C	0.37 ± 0.02	1.22 ± 0.02	1.60 ± 0.02	4.5 ± 0.1	1.88 ± 0.03	0.39 ± 0.04	[49]
D. vulgaris	Ni-A	0.32 ± 0.02	1.26 ± 0.02	1.58 ± 0.02	~ 4.6	1.90 ± 0.03	0.34 ± 0.04	[53]
D. vulgaris	Ni-B	0.36 ± 0.02	1.30 ± 0.02	1.66 ± 0.02	~ 4.2	1.98 ± 0.03	0.37 ± 0.04	[53]
D. gigas	Ni-C	0.4	1.2	1.6	4.5	1.9	0.4	[52]
D. gigas	Ni-A	0.4	1.2	1.6	4.4	1.9	0.4	[52]

role of the specific histidine residue in the catalytic cycle of H_2 oxidation. Obviously, the situation is different in less efficient catalysts like the H_2-sensing proteins.

Previous EPR analysis of the wild-type RH revealed the lack of both the Ni-A and Ni-B states in this protein. Incubation of the RH with H_2 resulted in the EPR-detectable Ni-C state of the reduced enzyme [19, 20]. These observations were confirmed by this study. In standard [NiFe] hydrogenases the proximal [4Fe-4S] cluster is usually reduced under 100% H_2 and the interaction of the nickel with the reduced cluster can be observed at low temperatures ($T < 50$ K) as a splitting in the EPR spectra [48]. A coupling of this type was neither observed for the wild-type RH nor for the RH (HoxC Q67H) protein in the present study.

In this study, EPR spectroscopy was also used to compare the electronic and geometric structure of the [NiFe] center of the wild-type RH with the RH (HoxC Q67H) protein. The g values of these two RH proteins are close to the g values reported for other hydrogenases (Table 3). The g_1 and g_2 values of the RH (HoxC Q67H) protein showed a small shift to larger values in comparison to the wild-type RH, whereas the g_3 value remained unchanged within error. Since the **g** tensor is a sensitive indicator for a metal center and its protein environment, the resemblance of the EPR signals of wild-type RH and RH (HoxC Q67H) protein indicates a very similar – although not identical – structure of the [NiFe] center.

The linewidth at the g_1 and g_2 components in the EPR spectrum of the RH (HoxC Q67H) protein is about 11 G. These values are remarkably reduced in comparison with the wild-type protein, where we obtained 16 G for g_1 and g_2. The decrease of the linewidth cannot be ascribed to different hyperfine couplings in the wild-type RH and the RH (HoxC Q67H) protein. This was confirmed by ENDOR measurements, which yielded very similar proton hfc values [49]. Thus, the change in linewidth is probably caused by a superposition of EPR signals from slightly different conformations (mircoheterogeneities) [50, 51] of the active center. The smaller linewidth of the EPR spectrum of the RH (HoxC Q67H) protein indicates a better defined structural situation of the active center. Obviously, the histidine residue provides an additional stabilization of the local structure of the [NiFe] cluster, probably caused by the formation of the hydrogen bond to the [NiFe] center detected in this study.

Using ESEEM and HYSCORE experiments we were able to detect coupling to a ^{14}N nucleus, which must be attributed to the exchanged residue His67 in the RH (HoxC Q67H) protein since the related interaction is absent in the wild-type RH. The ^{14}N quadrupole coupling observed for the RH (HoxC Q67H) protein is very similar to that observed in other hydrogenases [52, 53]. In Table 4 we have collected the reported frequencies of the ^{14}N transitions and the related quadrupole parameters for the different paramagnetic states of [NiFe] hydrogenases from *D. gigas* and *D. vulgaris* Miyazaki F. The e^2qQ/h values obtained for the RH (HoxC Q67H) protein were in good agreement with those reported for the [NiFe] hydrogenases from *D. gigas* and *D. vulgaris* Miyazaki F in the reduced state (Ni-C), whereas the sensitive asymmetry parameter η shows some deviation from the reported values for the two standard hydrogenases. The quadrupole parameters show only slight shifts for the various redox states, as expected for an ^{14}N nucleus in the same environment. The position of the double-quantum transition ν_{dq} displayed more pronounced changes. This can be explained by a change of the effective hyperfine coupling of the ^{14}N that depends on the amount of spin density transfer from the [NiFe] center to the histidine via the hydrogen bond.

The X-ray structure of the hydrogenase from *D. gigas* [2] indicated that the N(ϵ) of His72 is closest to the sulfur of Cys533, which carries a substantial part of the unpaired spin density [54]. Our DFT calculations performed on a model derived from the X-ray structure support the assignment of this coupling to N(ϵ) of His72. The calculated values for e^2qQ/h and η coincide with the experimentally determined values, if we assume that N(ϵ) and not N(δ) is protonated and forms a weak hydrogen bond with the sulfur of Cys533.

The calculated NQR parameters show a better correlation with the experimental data if we assume a smaller distance between the histidine and the cysteine residue for the RH (Q67H) protein than found in the standard hydrogenases (Fig. 7). The smaller distance indicates a stronger interaction and, furthermore, an additional stabilizing effect of the local structure. A better defined structure of the spin-carrying center was also suggested by our finding of different linewidths in the EPR spectra, arising from the wild-type RH and from the RH (Q67H) proteins (Fig. 4). Obviously, in the RH mutant protein the interaction between the histidine

and the cysteine locks the [NiFe] center in a well-defined tight conformation.

The question remains open of why the glutamine residue in the wild-type RH does not form a hydrogen bond comparable to that observed for the histidine residue of the RH (HoxC Q67H) protein. The proton of an imidazole nitrogen is more "acidic" than the protons of the amide group of a glutamine. Therefore, histidine is generally a better hydrogen donor than glutamine. In fact, hydrogen bonds donated by imidazole-nitrogens of histidine residues are often found in proteins, while hydrogen bonds donated by the amide group of glutamine residues are rare [55]. The occurrence of the hydrogen bond in the RH (HoxC Q67H) protein appears to be less relevant for the biological function of the H_2 sensor. Our results clearly show that this hydrogen bond arises from the introduced histidine residue. We can exclude the possibility that the observed coupling arises from a backbone nitrogen. The following NQR parameters for the ^{14}N nuclei of, for example, polyglycine, a model compound for the polypeptide backbone, were reported: $e^2qQ/h = 3.1$; $\eta = 0.76$ [56]. These values significantly differ from those obtained in this study for the RH proteins (see Table 4). Finally, our findings also provide an explanation for the observed ^{14}N quadrupole couplings in the [NiFe] hydrogenases of *D. gigas* [52] and *D. vulgaris* [53]. It was not possible to assign these couplings to a specific ^{14}N nucleus in these enzymes. Based on our results, however, it is likely that they derive from the N(ϵ) nucleus of the histidine residue of the L2 motif.

Acknowledgements Antonio L. De Lacey and Victor M. Fernandez (Madrid, Spain) are kindly acknowledged for carrying out the D_2/H^+ exchange experiments. We thank A. Strack (HU Berlin) for excellent technical assistance. This work was funded by the Deutsche Forschungsgemeinschaft (SFB 498, TP C1 and C2) and the Fonds der Chemischen Industrie.

References

1. Vignais PM, Billoud B, Meyer J (2001) FEMS Microbiol Rev 25:455–501
2. Volbeda A, Charon M-H, Piras C, Hatchikan EC, Frey M, Fontecilla-Camps JC (1995) Nature 373:580–587
3. Higuchi Y, Yagi T, Yasuoka N (1997) Structure 5:1671–1680
4. Happe RP, Roseboom W, Pierik AJ, Albracht SP, Bagley KA (1997) Nature 385:126
5. Pierik AJ, Roseboom W, Happe RP, Bagley KA, Albracht SP (1999) J Biol Chem 274:3331–3337
6. Carepo M, Tierney DL, Brondino CD, Yang TC, Pamplona A, Telser J, Moura I, Moura JJG, Hoffman BM (2002) J Am Chem Soc 124:281–286
7. Albracht SP (1994) Biochim Biophys Acta 1188:167–204
8. Cammack R (1999) Nature 397:214–215
9. Montet Y, Amara P, Volbeda A, Vernede X, Hatchikian EC, Field MJ, Frey M, Fontecilla-Camps JC (1997) Nat Struct Biol 4:523–526
10. Schink B, Schlegel HG (1979) Biochim Biophys Acta 567:315–324
11. Bernhard M, Benelli B, Hochkoeppler A, Zannoni D, Friedrich B (1997) Eur J Biochem 248:179–186
12. Schneider K, Schlegel HG (1976) Biochim Biophys Acta 452:66–80
13. Tran-Betcke A, Warnecke U, Böcker C, Zaborosch C, Friedrich B (1990) J Bacteriol 172:2920–2929
14. Schwartz E, Gerischer U, Friedrich B (1998) J Bacteriol 180:3197–3204
15. Lenz O, Friedrich B (1998) Proc Natl Acad Sci USA 95:12474–12479
16. Kleihues L, Lenz O, Bernhard M, Buhrke T, Friedrich B (2000) J Bacteriol 182:2716–2724
17. Elsen S, Colbeau A, Chabert J, Vignais PM (1996) J Bacteriol 178:5174–5181
18. Black LK, Fu C, Maier RJ (1994) J Bacteriol 176:7102–7106
19. Pierik AJ, Schmelz M, Lenz O, Friedrich B, Albracht SPJ (1998) FEBS Lett 438:231–235
20. Bernhard M, Buhrke T, Bleijlevens B, De Lacey AL, Fernandez VM, Albracht SP, Friedrich B (2001) J Biol Chem 276:15592–15597
21. Yanisch-Perron C, Viera J, Messing J (1985) Gene 33:103–119
22. Simon R, Priefer U, Pühler A (1983) Bio/Technology 1:784–791
23. Chen B, Przybyla AE (1994) BioTechniques 17:657–659
24. Lenz O, Schwartz E, Dernedde J, Eitinger M, Friedrich B (1994) J Bacteriol 176:4385–4593
25. Bernhard M, Schwartz E, Rietdorf J, Friedrich B (1996) J Bacteriol 178:4522–4529
26. Towbin H, Staehelin T, Gordon J (1979) Proc Natl Acad Sci USA 76:4350–4357
27. Zimmer D, Schwartz E, Tran-Betcke A, Gewinner P, Friedrich B (1995) J Bacteriol 177:2373–2380
28. Miller JH (1972) Experiments in molecular genetics. Cold Spring Harbor Laboratory Press, Cold Spring Harbor, NY
29. Lowry OH, Rosebroug NJ, Farr AL, Randall RJ (1951) J Biol Chem 193:265–275
30. Fahnenschmidt M (2000) PhD thesis. Technische Universität Berlin, Germany
31. Höfer P, Grupp A, Nebenführ H, Mehring M (1986) Chem Phys Lett 132:279–282
32. Gemperle C, Aebli G, Schweiger A, Ernst RR (1990) J Magn Reson 88:241–256
33. Flanagan HL, Singel DJ (1987) J Chem Phys 10:5606–5616
34. Dikanov SA, Tsvetkov JD (1992) Electron spin echo envelope modulation (ESEEM). CRC Press, Boca Raton
35. Atherton NM (1993) Principles of electron spin resonance. Ellis Horwood PTR Prentice Hall, New York
36. Mims WB, Peisach J (1978) J Chem Phys 69:4921–4930
37. Lucken EAC (1969) Nuclear quadrupole coupling constants. Academic Press, London
38. Frisch MJ, Trucks GW, Schlegel HB, Gill PMW, Johnson BG, Robb MA, Cheeseman JR, Keith T, Petersson GA, Montgomery JA, Raghavachari K, Al-Laham MA, Zakrzewski VG, Ortiz JV, Foresman JB, Peng CY, Ayala PY, Chen W, Wong MW, Andres JL, Replogle ES, Gomperts R, Martin RL, Fox DJ, Binkley JS, Defrees DJ, Baker J, Stewart JP, Head-Gordo M, Gonzalez C, Pople JA (1995) Gaussian 94, revision B.3. Gaussian, Pittsburgh, Pa
39. Becke A (1993) J Chem Phys 98:5648–5652
40. Foresman JB (1996) In: Frisch MJ (ed) Exploring chemistry with electronic structure methods. Gaussian, Pittsburgh, Pa
41. Petersson GA, Bennet A, Tensfeldt TG, Al-Laham MA, Shirley WA, Mantazaris J (1988) J Chem Phys 89:2193–2218
42. Bailey WC (2000) Chem Phys 252:57–66
43. Müller A, Tscherny I, Kappl R, Hatchikian EC, Hüttermann J, Cammack R (2001) J Biol Inorg Chem 7:177–194
44. van der Zwaan JW, Coremans JMCC, Bouwens ECM, Albracht SPJ (1990) Biochim Biophys Acta 1041:101–110
45. Bailey WC (1998) Chem Phys Lett 292:71–74
46. Latosinska JN, Koput J (2000) Phys Chem Chem Phys 2:145–150
47. Massanz C, Friedrich B (1999) Biochemistry 38:14330–14337
48. Teixeira M, Moura I, Xavier AV, Huynh BH, DerVartanian DV, Peck HD, Le Gall J, Moura JJG (1985) J Biol Chem 260:8942–8950
49. Brecht M (2001) PhD thesis. Technische Universität Berlin, Germany

50. Hagen WR, Hearshen DO, Harding LJ, Dunham WR (1985) J Magn Reson 61:220–232
51. Hagen WR, Hearshen DO, Harding LJ, Dunham WR (1985) J Magn Reson 61:233–244
52. Chapman A, Cammack R, Hatchikian CE, McCracken J, Peisach J (1988) FEBS Lett 242:134–138
53. Brecht M, Stein M, Trofanchuk O, Lendzian F, Bittl R, Higuchi Y, Lubitz W (1998) In: Ziessow D, Lendzian F, Lubitz W (eds) Magnetic resonance and related phenomena, vol II. Technische Universität Berlin, pp 818–819
54. Stein M, Lubitz W (2001) Phys Chem Chem Phys 3:2668–2675
55. McDonald IK, Thornton JM (1994) J Mol Biol 238:777–793
56. Bosch MK, Gast P, Hoff AJ, Spoyalov AP, Tsvetkov YD (1995) Chem Phys Lett 239:306–312
57. Stein M (2001) PhD thesis. Technische Universität Berlin, Germany